FINE-TUNING COMPONENTS OF INVERSE-CALIBRATED, THERMAL-BASED REMOTE SENSING MODELS FOR EVAPOTRANSPIRATION

Richard G. Allen, Professor
Jeppe Kjaersgaard, Asst. Professor
Magali Garcia, Visting Professor
University of Idaho – Kimberly Research and Extension Center
Kimberly, ID 83341
rallen@kimberly.uidaho.edu
jeppek@kimberly.uidaho.edu
mgarcia@kimberly.uidaho.edu

ABSTRACT

Several surface energy balance models are now routinely operated to produce ET products on an operational basis for use in water resources and water rights management. These models generally determine evapotranspiration (ET) at local, Landsat resolution scales, and thermal images are a vital input to these processes. Two of these models, METRIC and SEBAL, use calibration using inverse modeling at extreme conditions (*CIMEC*) to derive unique calibrations that change each image. Often the focus of the calibration is toward relative dry and wet conditions within agricultural areas due to the importance of calibrations fitting this land use. Often, a satellite image contains land-use features other than agriculture where soil characteristics, such as crusting and delamination, impact surface temperature and soil heat flux density differently than for the tilled agricultural soils used in the *CIMEC* calibrations. In these instances sensible heat flux, which is used to estimate ET as a residual, can be overstated. An assortment of techniques are discussed in this paper for modifying the vegetation-based estimates for soil heat flux density under varying land-use classes, for modifying the estimate for near surface air temperature gradient, for applying some excess aerodynamic resistances for sparse desert vegetation such as sage brush, and for modifying wind and aerodynamic conditions in mountains.

INTRODUCTION

Evapotranspiration (ET) is highly variable in both space and time. It is variable in space due to the wide spatial variability of precipitation, hydraulic characteristics of soils, and vegetation types and densities. It is variable in time due to variability of climate and development or senescence of vegetation. Satellite images provide an excellent means for determining and mapping the spatial and temporal structure of ET. The METRIC*tm* model developed at the University of Idaho (Allen et al., 2002, 2005, 2007a,b) calculates ET via a surface energy balance that is driven by satellite images containing both short wave and thermal information. The advantage of ET by energy balance is that actual ET is obtained rather than potential ET. Actual ET can be less than potential due to effects of water shortage, low irrigation uniformity, salinity of soil and water, sparse vegetation, waterlogging and disease. Another advantage of ET by energy balance is that a specific classification and identification of crop type by field is not generally required. Requirement of a crop specific classification can significantly increase costs of ET mapping.

METRIC*tm* calculates ET through a series of computations that estimate net surface radiation, soil heat flux, and sensible heat flux to the air. Details of calculations are given in Allen et al. (2007a). By subtracting the soil heat flux and sensible heat flux from the net radiation at the surface, a "residual" energy flux can be estimated that represents the energy consumed by evapotranspiration (i.e. energy that is used to convert liquid water into water vapor). METRIC*tm* is designed to produce high quality and accurate maps of ET for focused regions smaller than a few hundred kilometers in scale and at high resolution. The primary and generally preferred satellite image for processing is that from Landsat due to the high resolution of short-wave (30 m) and thermal (60 – 120 m) information that permits detailed ET from individual agricultural fields and narrow riparian systems along streams to be viewed. This contrasts with some remote sensing models that are more general based and are designed for routine application over large regions (for example over subcontinents). The narrowed focus of METRIC*tm* is intended to provide more accurate estimates of ET and at higher resolution (~30 m) as compared to more general models. The narrowed focus does come at a cost, however, in the requirement for intelligent experts having good background in energy balance and radiation physics and adequate knowledge of vegetation characteristics as well as the requirement for high quality hourly (or shorter) weather data.

Internal calibration of the energy balance in METRIC*tm* utilizes ground-based reference ET (ET_r) to "tie-down" the derived energy balance. Use of quality controlled ET_r is considered to improve accuracy of daily and longer period ET estimates and provides relatively seamless congruency with traditional crop coefficient x ET_r approaches that use ET_r as their basis. A primary difference between METRIC*tm* and SEBAL is METRIC's greater reliance on ground-based reference ET for calibration. Reliance on weather data can be a disadvantage when quality weather data are not available.

Sensible heat flux is the rate of heat loss to the air by convection and conduction, due to a temperature difference. It is estimating in METRIC using a one-dimensional, aerodynamic, temperature gradient based equation for heat transport that utilizes a temperature difference, dT between two near surface heights, both suspended above the surface:

$$H = \frac{\rho\, c_p\, dT}{r_{ah}} \tag{1}$$

where H is the sensible heat flux density, ρ is air density, c_p is air specific heat, dT (K) is the temperature difference ($T_1 - T_2$) between two heights (z_1 and z_2), and r_{ah} is the aerodynamic resistance to heat transport (s/m) between z_1 and z_2. METRIC calibrates the dT estimating function for each image and date using inverse modeling of extreme conditions (*CIMEC*). Often the focus of the calibration is toward relative dry and wet conditions within agricultural areas. Agricultural areas are generally selected for extreme condition calibration because of their importance in water resources consumption and management and because vegetation in these systems is generally more uniform and the energy balance "better behaved." The *CIMEC* process is applied by inverting Eq. 1 for dT after determining the value for H by inversion of the energy balance equation where $H = R_n - G - LE$ where R_n is net radiation, G is soil heat flux density and LE is latent heat flux density, at extreme conditions of nearly potential LE and nearly zero LE. Locations are identified in each satellite image where these conditions apply. The estimation of LE is done for the wetter condition using the reference ET_r computed from quality controlled hourly weather data and the estimation of LE for the drier condition is done using a daily soil water balance – evaporation model that is also weather data driven and that estimates any residual evaporation from a bare soil caused by antecedent rainfall. The use of the *CIMEC* approach imbeds any systematic biases from the estimates for R_n, G, surface temperature, T_s, and r_{ah} into the dT parameter and thus into the estimate for H. This bias in the H estimate is, however, removed from the resulting LE estimate by nearly perfect compensation upon calculating LE as a residual of the energy balance:

$$LE = R_n - G - H \tag{2}$$

METRIC*tm* calculates dT for each image pixel by assuming a linear relationship between dT and T_s that is calibrated to each satellite image:

$$dT = b + aT_{s\ dem} \tag{3}$$

where b and a are the calibration coefficients, and T_s is surface temperature from the satellite adjusted to a common, arbitrary elevation datum using a specified lapse rate. The adjustment to $T_{s\ dem}$ compensates for change in T_s with elevation that is related more to warming or cooling of air masses with change in elevation rather than with change in surface energy balance and evaporation. The linearity of the dT vs. T_s function is a major assumption of METRIC*tm* and its basis SEBAL (Bastiaanssen et al. 1998). Research by Bastiaanssen (1995) and others and comparisons of final ET estimates over a range of dT values by the University of Idaho at Kimberly (Tasumi et al., 2005; Allen et al., 2007a), indicate that this assumption fits a wide range of conditions.

The following sections describe 'refinements' and 'fine-tuning' done to METRIC applications to 'coax' out what we hope to be more accurate maps (images) of evapotranspiration. This fine-tuning is done in an operational, engineering sense, where routine applications are made in a variety of areas, and adjustments must be straightforward and robust over large changes in landscape. These approaches may or may not be helpful with other energy balance approaches.

COMPUTATION OF RADIATION COMPONENTS

The METRIC model is intended to be applied on a relatively rapid and operational basis and often by ET experts who may not necessarily have expertise in radiation and atmospheric physics. Therefore, rather than require users to apply atmospheric correction to images requiring use of radiosondes and detailed models such as MODTRAN, METRIC applies a relatively simple, but robust calculation for at-surface reflectance on a band-by-band basis following Tasumi et al. (2008) as:

$$\rho_{s,b} = \frac{\rho_{t,b} - C_b(1-\tau_{in,b})}{\tau_{in,b} \cdot \tau_{out,b}} \tag{4}$$

where $\rho_{t,b}$ is at-satellite reflectance for band "b", and $\tau_{in,b}$ and $\tau_{out,b}$ are narrowband atmospheric transmittances for incoming solar radiation and for surface reflected shortwave radiation. Coefficient C_b was developed to estimate path radiance for both Landsat and MODIS images. Values are given in Allen et al. (2007a) and Tasumi et al (2008). Tasumi et al. (2008) found good estimation of specific band transmittances using an equation similar in form and structure to that used by Majumdar et al. (1972), Allen (1996) and Allen et al. (1998) for general broad-spectrum solar transmittance:

$$\tau_{in,b} = C_1 \exp\left[\frac{C_2 \cdot P_{air}}{K_t \cos\theta_h} - \frac{C_3 W + C_4}{\cos\theta_h}\right] + C_5 \tag{5}$$

where C_1 to C_5 are calibration constants, K_t is a unitless "clearness" coefficient $0 < K_t <= 1.0$ where $K_t = 1.0$ for clean air and $K_t = 0.5$ for turbid, dusty or polluted air, θ_h is the solar zenith angle (radians), P_{air} is air pressure (kP_a), and W is precipitable water in the atmosphere (mm). Usually K_t is set equal to 1.0 for applications to agricultural areas where air is generally clean.

Outgoing narrowband transmittance, $\tau_{out,b}$, is approximated the same way as incoming transmittance, but where the solar zenith angle is set to zero, representing the vertical radiation path length between the land surface and the sensor of Landsat pointing at nadir. Therefore:

$$\tau_{out,b} = C_1 \exp\left[\frac{C_2 \cdot P_{air}}{K_t \cdot 1} - \frac{C_3 W + C_4}{1}\right] + C_5 \tag{6}$$

At surface albedo is computed from the band reflectances using weighting of Tasumi et al. (2008). The surface albedo determined using Eq. 4-6 is sufficiently accurate for application of the energy balance within the METRIC context due to the calibration-bias cancellation strategy imbedded in the *CIMEC* approach.

Similarly, a general atmospheric correction is made to the thermal radiance emitted from the surface (R_c) calculated following Wukelic et al. (1989) where:

$$R_c = \frac{L_6 - R_p}{\tau_{NB}} - (1 - \varepsilon_{NB})R_{sky} \tag{7}$$

where L_6 is the spectral radiance of the thermal band (band 6 for Landsat) ($W/m^2/sr/\mu m$), R_p is the path radiance in the 10.4 – 12.5 μm band ($W/m^2/sr/\mu m$), R_{sky} is the narrow band downward thermal radiation from a clear sky ($W/m^2/sr/\mu m$), and τ_{NB} is the narrow band transmissivity of air (10.4 – 12.5 μm). Units for R_c are $W/m^2/sr/\mu m$.

Values for R_p and τ_{NB} usually require the use of an atmospheric radiation transfer simulation model such as MODTRAN and radiosonde profiles representing the image and date. However, based on multiple MODTRAN runs conducted for a range of image dates during spring, summer and fall in southern Idaho, Allen et al. (2007a) suggested using $R_p = 0.91$, $\tau_{NB} = 0.866$ and $R_{sky} = 1.32$ for low aerosol conditions (similar to those in the western US). Because METRIC*tm* tempers the dT function to the T_s data calculated for an image, the impact of any bias in T_s on final ET values is generally small, especially for areas having low and high values of ET that are near the *CIMEC* calibration conditions. Errors may be larger for midrange ET values, but are generally less than a few percent. A comparison of the consistency of the general T_s calibration in southern Idaho based on MODTRAN correction and the above simplified coefficients is shown in Fig. 1.

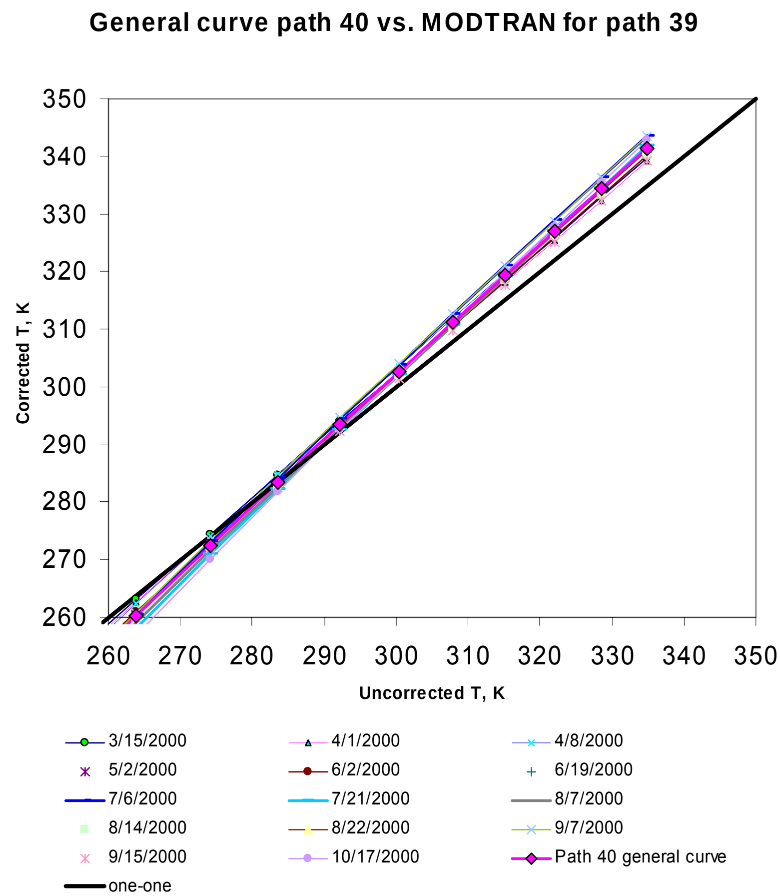

.

Figure 1. Comparison of corrected T_s based on MODTRAN analyses (Trezza, 2002) and uncorrected T_s (using $R_p = 0$, $\tau_{NB} = 1$ and $R_{sky} = 0$). The estimates using $R_p = 0.91$, $\tau_{NB} = 0.866$ and $R_{sky} = 1.32$ (path 40 general curve) are shown to approximate relationships for all dates.

FINE TUNING OF METRIC COMPONENTS

Because of nature's complexity and heterogeneity, individual components of energy balance methods such as METRIC require occasional 'fine-tuning' to produce improved estimates of ET. These occasions may be when special focus is placed on desert systems having weathered, crusted soils or sparse vegetation and on mountain areas having high ranges in elevation. Fine tuning of METRIC^{tm} applications often includes the following:

- Modification of soil heat flux computation for desert soils (due to lamination, dryness, or excessive soil temperatures)
- Placement of limits on dT for extreme desert conditions
- Customized lapse correction for the dT function
- Excess aerodynamic resistance for sparse desert vegetation

Soil Heat Flux (G)

Soil heat flux is the rate of heat storage into the soil and vegetation due to conduction. METRIC^{tm} provides an open platform for how G is estimated, but generally estimates the ratio G/R_n using an empirical equation developed by Bastiaanssen (1995) representing values near midday:

$$G/R_n = (T_s - 273.15)\,(0.0038 + 0.0074\,\alpha)\,(1 - 0.98\,NDVI^4) \quad (7)$$

where T_s is the surface temperature (K), α is the surface albedo, and NDVI is the Normalized Difference Vegetation Index (at top of atmosphere). G is calculated by multiplying G/R_n by the value estimated for R_n. An alternative equation sometimes used developed by Tasumi et al., (2003) for irrigated crops near Kimberly, Idaho:

$$G / R_n = 0.05 + 0.18e^{-0.521LAI} \qquad (LAI \geq 0.5) \qquad (8a)$$

$$G / R_n = 1.80(T_s - 273.15)/R_n + 0.084 \qquad (LAI < 0.5) \qquad (8b)$$

where LAI is the Leaf Area Index. Both Equations 7 and 8a,b estimate G measured for irrigated crops near Kimberly, Idaho relatively accurately (Tasumi et al., 2003) and represent G/R_n for agricultural soils that have been tilled within the last few hundred days of the image date and thus have good tilth without a large amount of cracking or delamination. Eq. (7) suggests that G/R_n increases with increasing albedo (indicative of bright bare soils that often have high reflection) and decreases with increasing vegetation (due to shading by the canopy). Eq. (8a) suggests that G/R_n decreases with increasing leaf area, for the same reason, and Eq. (8b) suggests that for bare or nearly bare soil, G increases in proportion to surface temperature.

Soil heat flux is a difficult term to evaluate and care should be used in its estimation. In some applications of METRIC*tm*, the G function is adjusted during application to desert soils to account for delamination and differences in porosity, structure and other effects that cause these soils to deviate from their agricultural counterparts. The upper soil layers in cropped agricultural fields are likely to be disturbed on a routine basis (every few hundred days or less) by tillage, emerging plants and plant roots. This disturbance tends to promote a somewhat uniform and contiguous vertical soil structure within the upper ten cm, so that delamination, crust formation, cracking etc. are largely absent.

For undisturbed, dry desert soils, where vegetation is sparse and the upper soil layer is largely undisturbed, a thin crust often forms at the soil surface. This crust may be partially delaminated from the soil below and thus separated by an air gap. Freeze-thaw cycles and swelling clay minerals can also cause differences in texture, structure and bulk density in the upper ten cm of the soil. Any lamination and delamination will likely reduce G, as energy transfer by conduction from the crust to the immediate underlying soil layers is reduced. The dryness of the upper soil also reduces G, as water increases the thermal conductivity of soil. The G function that is used in METRIC was derived from agricultural soils that contained moderate amounts of soil water. Hence, this function may overestimate G for dry, desert soils, even under conditions of similar structure. If there has been snowmelt or rain events prior to the capture time of the image, the soil may contain residual moisture and the effects of delamination of upper soil layers may be less pronounced.

To adjust for applications to desert soils, the G that is computed using Eq. 7 or 8a,b is sometimes reduced for pixels having surface temperature beyond the temperature of dry, bare agricultural pixels, denoted as T_{s_dry}, as:

$$G_{adj} = G - 5(T_{s\,dem} - T_{s\_dry\ dem}) \quad \text{for } T_{s\,dem} > T_{s\_dry\,dem} \qquad (9)$$
$$G_{adj} = G \quad \text{otherwise}$$

where G has units of W/m^2 and T_s is in K, and G is from Eq. 7 or 8a,b. The philosophy behind Eq. 9 is that bare soil that has T_s greater than that of T_{s_dry} must be hotter partially because of reduced heat flux into the soil (in addition to any other causes). Eq. 9 was derived during applications of METRIC to soils in New Mexico and southern Idaho as a means to reduce negative values frequently derived for ET. The values for T_s and T_{s_dry} in Eq. 9 are lapse adjusted for elevation using a DEM map.

Applications in Mountains

For application to mountainous areas where there is significant relief and a wide range of slopes and aspects, the METRIC*tm* 'Mountain Model' version includes computations for influence of slope, aspect, and elevation on solar and thermal radiation estimates (Allen et al. 2006, 2007a) in addition to application of lapse correction in the function for dT. In addition, estimated air flow (wind speed) and aerodynamic roughness over mountainous areas is adjusted to consider effects from orthographic drainage of air caused by cooling, the acceleration of air streams passing over mountains due to the venturi effect, and the impacts of drag due to undulating topography, all of which combine to make wind speed prediction difficult and complicated. Atmosheric transmissivity values are computed uniquely for each pixel as a function of the elevation.

Lapse Correction. Generally, air temperature decreases from 5 to 10ºC for each 1 km elevation increase under neutral stability conditions. Since surface temperatures are in strong equilibrium with air temperature, one can usually observe similar decreases in surface temperature. A "lapsed" (artificial) surface temperature map is created for purposes of computing dT by assuming that the rate of decrease in surface temperature due to elevation increase is the same as that for a typical air mass. The elevation data are provided by DEM. The DEM corrected surface temperature is calculated as:

$$T_{s\_dem} = T_s + C_{lapse}\Delta z \qquad (10)$$

where C_{lapse} is the lapse rate, Δz is the elevation of each pixel minus the elevation of an arbitrary datum (m) in the image where T_{s_dem} is specified to equal T_s. The term Δz is positive if the elevation of a pixel is higher than the datum. The adiabatic lapse rate for saturated air is about 6.5 K/1000 m. The adiabatic lapse rate for dry air is about 10 K/1000 m. The moist rate is lower due to the heating of air during vapor condensation. A lapse rate is generally custom fit to an image and date by plotting T_s of a number of randomly selected pixels against elevation. Visually determined slopes of upper and lower bounds are used to determine mean apparent lapse for the image (fig. 2). Often, the standard saturated lapse rate of 6.5 K/km applies.

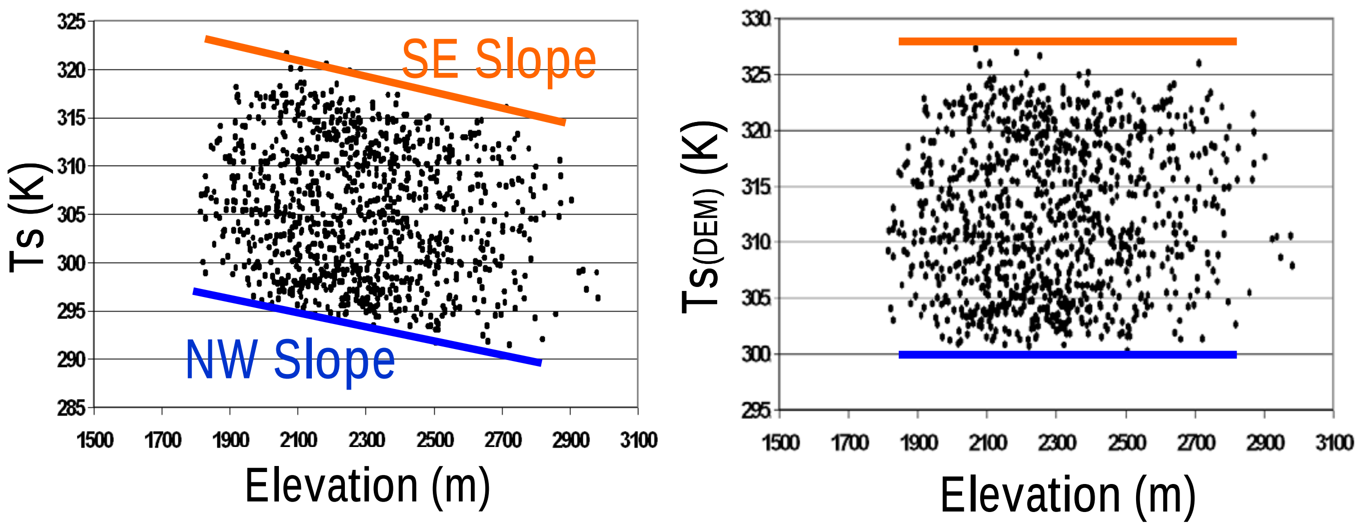

Figure 2. T_s and T_{s_dem} for the same locations sampled from relatively flat areas in a mountainous region, where a 6.5 K/1000 m lapse rate was applied. The large range in T_s within any elevation range is due primarily to variation in vegetation (from Tasumi, 2003).

Momentum Roughness Length for Mountainous Areas. The momentum roughness length (z_{om}) is initially computed using a land use map and LAI. It is then adjusted for terrain roughness (fig. 3) using slope as a parameter using an equation developed during applications in southern Idaho mountains:

$$z_{om(mnt)} = z_{om} \times [1 + (slope_{deg} - 5)/20] \quad \text{for } slope_{deg} \geq 5° \qquad (11)$$

$$z_{om(mnt)} = z_{om} \quad \text{otherwise}$$

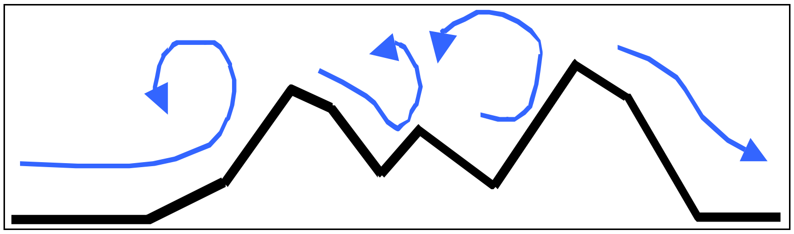

Figure 3. Schematic showing terrain roughness impacts in mountains.

Adjustment of Wind Speed. In METRIC, a wind velocity 'surface' is established at 200 meters height (u_{200}), representing a blended layer. This wind speed is then extrapolated to the surface using roughness and stability behavior for each pixel. In mountain applications, u_{200} is also adjusted for elevation. Elevation effects on wind speed are complicated and difficult to quantify. They are generally a function of wind direction, which is unknown, and location in the terrain, where Venturi effects as well as wind sheltering occur (Fig. 4). On average, wind speeds are generally greater in mountainous terrain. A general mountain wind speed adjustment coefficient (ϖ) developed during University of Idaho applications is used to increase u_{200} in mountainous terrain:

$$\varpi = 1 + 0.1[\ (\{\text{Elevation} - \text{Elevation}_{\text{station}}\}/1000)] \qquad (12)$$

where Elevation is the elevation of a pixel and $\text{Elevation}_{\text{station}}$ is the elevation where the wind speed is measured. u_{200} for each pixel is adjusted by multiplying it by ϖ.

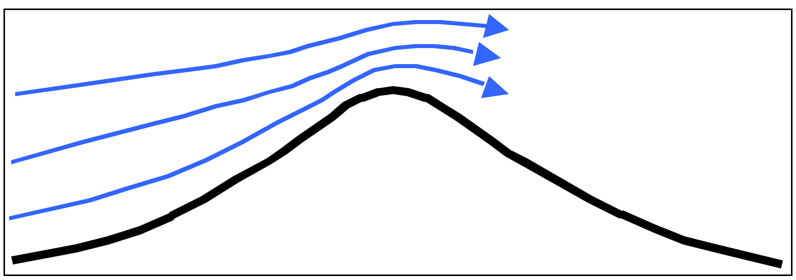

Figure 4. Schematic showing acceleration of air speed due to the Venturi effect in mountains

Desert Systems

In some applications of METRIC, evapotranspiration computed for desert areas can become systematically negative. This occurs because METRIC is generally calibrated to produce nearly zero ET for bare, agricultural locations. Higher surface temperature in desert areas causes the internal energy balance to overestimate sensible heat flux and thus produce negative values for ET. This has been the case for images processed in south central Idaho and in New Mexico. Fine tuning adjustments to METRIC to desert systems has at time included the use of an excess resistance to compensate for this.

Excess resistance. METRIC can systematically overestimate sensible heat and underestimate ET for some desert systems. A plausible cause for such behavior is the influence that sage brush and tall grass vegetation on surface temperature, where the sparse vegetation systems effectively protect the land surface from mechanical heat transport (i.e., wind), but are sparse enough to permit the penetration of incoming solar radiation that heats the soil surface (Figure 5). This combination of permitting solar radiation penetration but inhibiting wind penetration makes the surfaces of some desert areas sensed by the satellite extremely hot. Therefore, METRIC assigns, via the linear dT function, large values to the sensible heat flux density by assuming large vertical air-temperature gradients and strong buoyancy of air corresponding to the extreme surface temperature according to Monin-Obukhov similarity theory.

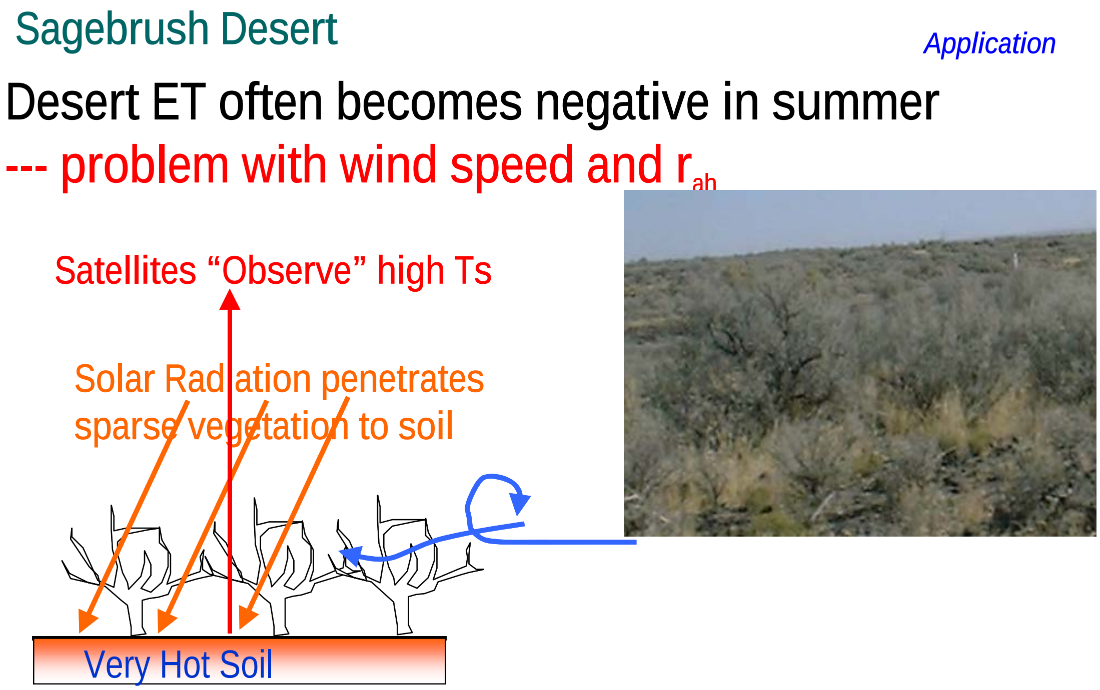

Figure 5. Schematic showing soil heating by penetration of solar radiation beneath a sparse sagebrush canopy, but shielding of wind by the canopy.

In METRIC, an empirical correction has been explored where we add an extra resistance, r_{extra} , to the calculation of sensible heat flux. Incorporating the extra resistance, the estimated H equation becomes:

$$H = \frac{\rho_{air} c_p dT}{r_{ah} + r_{extra}} \qquad (13)$$

An extra resistance function was developed based on H measured by an eddy covariance-sonic system located in a sagebrush desert site. The resistance was determined by inverting Eq. 13 for r_{extra}. Figure 6 shows plots of estimated r_{extra} vs windspeed on 12 Landsat image dates from mid to late summer in 2000 and 2003. Two typical desert areas were selected from each image, and each point in the figure represents the average value from a selected desert area. The regression equation by this analysis is:

$$r_{extra} = 0.0130u^3 - 0.4351u^2 + 4.2748u - 8.2835 \qquad r^2{=}0.61,\ n{=}24 \qquad (14)$$

where r_{extra} is in s/m, and u is windspeed at 200m in m/s.

Equation 14 is limited to values of wind speed less than 15 m s^{-1} (beyond 15 m s^{-1}, the correction is constrained to r_{extra} = 2 s m^{-1}). A lower limit of r_{extra} = 0 is imposed when wind speed is less than 2.6 m s^{-1}. The value for r_{extra} is small at low wind speeds because the heat transfer is then dominated by buoyancy and is thus essentially independent of surface roughness and shielding by vegetation. At high values of wind speed, the required value for r_{extra} is again small because of more effective mechanical penetration of wind to the soil surface within the sparse vegetation and subsequent surface cooling. The cooler surfaces result in calculation of smaller values for dT and thus H. It is the middle range of wind speed (3 to 10 m s^{-1} at 200 m height) that requires the most adjustment via r_{extra} due to the larger impact of sheltering of the surface. The mechanism for generating a universal trend between r_{extra} and windspeed is complicated because of the interdependencies between friction velocity (u_*), r_{ah} and the air temperature gradient (dT), as air-stability correction affects all of these terms.

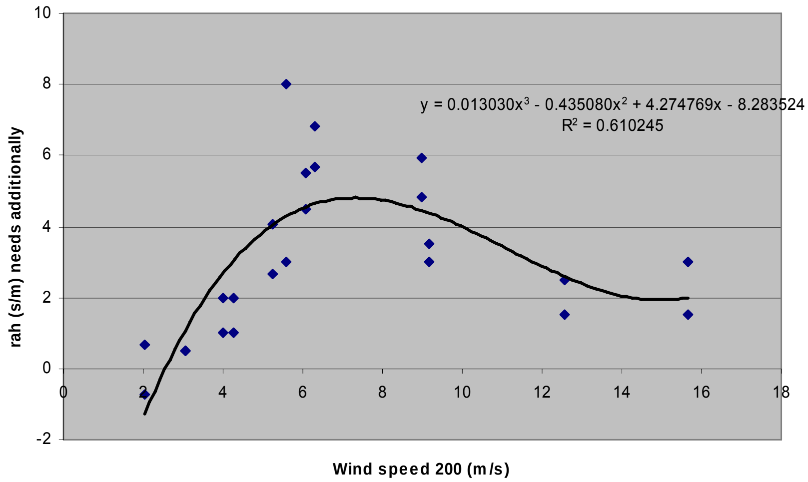

Figure 6. Values for extra resistance that cause ET at average desert locations to be zero in mid to late summer.

Reduction in the Slope of the dT = aT$_s$ + b function. Some desert areas of images can have T_s values that are significantly above that of the hot pixel, even under bare conditions. When sagebrush or other covers are present, the increase in T_s may be attributable to (and solved by) the excess resistance term described previously. Under bare soil conditions, however, the increase in T_s is more likely due to impacts of delaminated soils or desert soils having little structure, or, in agricultural conditions, elevated T_s may occur in fields having an insolating mulch or straw layer at the surface.

Under these conditions, the increased T_s beyond T_s of a dry, bare tilled field, T_{s_dry} causes the dT to be overestimated, since an increase in dT that is substantially beyond that determined for the $T_{s\ dry}$ condition is not physically possible. This is because at the $T_{s\ dry}$ condition, essentially all R_n-G is convected away via H, so that H approaches an upper limit for this available energy condition. No increase in the temperature gradient, dT, is expected beyond this H, even when the surface temperature increases beyond $T_{s\ dry}$. Therefore, in practice, the slope (a) may be reduced when $T_s > T_{s\ dry}$. In applications of METRIC in Idaho and New Mexico, the values for parameter a have been reduced to only 25% of the computed value when $T_s > T_{s\ dry}$ for the temperature segment that is beyond $T_{s\ dry}$. In practice, because the amounts of available energy (R_n – G) vary between agricultural and nonagricultural systems due to differences in soil reflectivity and structure, the threshold at which the slope of the dT function is reduced may be best set at some threshold value, $T_{s\ threshold}$ that is a few degrees hotter than that of the $T_{s\ dry}$. In equation form:

$$\begin{aligned} dT &= b + a\,T_{s\,dem} \quad \text{if } T_{s\,dem} \le T_{s\,threshold\,dem} \\ dT &= b + a\,T_{s\,threshold\,dem} + \frac{a}{4}\left(T_{s\,dem} - T_{s\,threshold\,dem}\right) \quad \text{if } T_{s\,dem} > T_{s\,threshold\,dem} \end{aligned} \tag{15}$$

where $T_{s\ dem}$ is the T_s for any pixel, corrected for elevation and $T_{s\ threshold\ dem}$ is the T_s for the hot threshold condition, corrected for elevation, where the break in slope occurs. An example of Eq. 15 is shown in Figure 7. The $T_{s\ threshold\ dem}$ is estimated from the $T_{s\ hot\ dem}$ (T_s of the hot calibration pixel) after that temperature has been adjusted to a fully dry condition, if needed:

$$T_{s\_threshold\_dem} = T_{s\_dry\_dem} + K_{offset} \tag{16}$$

where $T_{s\_dry\_dem}$ is the temperature equivalent associated with the hot pixel used in calibrating METRIC, but is adjusted, if needed, using Eq. 17 to represent a completely dry surface condition. The K_{offset} is a temperature offset to $T_{s\ dry\ dem}$, and is recommended to be about 2 K.

In instances where the 'hot' calibration pixel of METRIC has some residual evaporation due to antecedent rainfall or residual evaporation from tillage, past irrigation, etc. (so that the $ET_{hot} > 0$), $T_{s\_dry\_dem}$ will exceed the $T_{s\_hot\_dem}$ used during METRIC calibration, and is estimated as

$$T_{s\_dry\_dem} = T_{s\_hot\_dem} + ET_rF_{hot}\left(\frac{T_{s\_hot\_dem} - T_{s\_cold\_dem}}{ET_rF_{cold} - ET_rF_{hot}}\right) \tag{17}$$

where $T_{s\_hot\_dem}$ and $T_{s\_cold\_dem}$ are the lapse corrected surface temperatures at the hot and cold pixels, and ET_rF_{hot} and ET_rF_{cold} are the ET_rF assigned to the hot and cold pixels in METRIC during the *CIMEC* calibration. ET_rF represents the ET of an pixel expressed as a fraction of reference ET, where reference ET (ET_r) is computed from quality-controlled hourly (or shorter period) weather data. In the case of METRIC, ET_r is computed using the ASCE-EWRI (2005) standardized Penman-Monteith equation fitted to an alfalfa reference.

The application of Eq. 15 tends to 'tone down' the dT under the very hot surface temperatures experienced under some desert conditions and constrains the sensible heat flux estimate. The value for dT is not completely limited to that estimated for the hot pixel condition, since some pixels may have available energy (R_n – G) that exceeds that for the hot pixel. The user needs to iteratively examine the impact of application of the excess resistance and Eq. 15 to determine if both, or only one, or none of these extensions is required for the particular image, area and land-use.

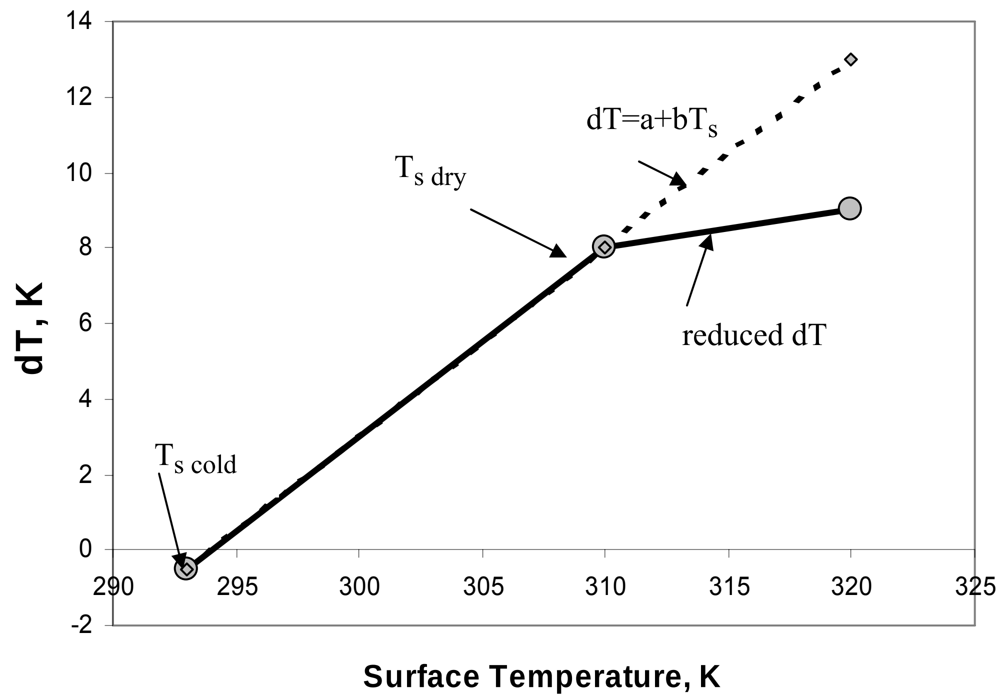

Figure 7. Schematic showing the application of Eq. 15 to reduce dT for T_s greater than that for a hot threshold condition.

REFERENCES

Allen, R.G. 1996. "Assessing integrity of weather data for use in reference evapotranspiration estimation." *J. Irrig. and Drain. Engrg.*, ASCE. Vol. 122(2): 97-106.

Allen, R. G., Pereira, L., Raes, D., and Smith, M. 1998. *Crop Evapotranspiration*, Food and Agriculture Organization of the United Nations, Rome, Italy. ISBN 92-5-104219-5. 300 p.

Allen, R.G., A. Morse, M. Tasumi, R. Trezza, W. Bastiaanssen, J.L. Wright, and W. Kramber. 2002. Evapotranspiration from a Satellite-Based Surface Energy Balance for the Snake Plain Aquifer in Idaho. Proceedings of the 2002 USCID/EWRI Conference, San Luis Obispo, July 9-12, 2002. p. 167-178.

Allen, R.G., M.Tasumi, A.T. Morse, and R. Trezza. 2005. A Landsat-based Energy Balance and Evapotranspiration Model in Western US Water Rights Regulation and Planning. *J. Irrigation and Drainage Systems* 19(3-4): 251-268.

Allen, R.G, Trezza, R, and Tasumi, M. 2006. Analytical integrated functions for daily solar radiation on slopes. *Agric For Meteorol* 139: 55-73.

Allen, R.G., M.Tasumi and R. Trezza. 2007a. Satellite-based Energy Balance for Mapping Evapotranspiration with Internalized Calibration (METRIC) -- Model. *J. Irrig. and Drain. Engrg,* ASCE 133(4), 380-394.

Allen, R.G., M.Tasumi, A. Morse, R. Trezza, W. Kramber, I. Lorite-Torres, C.W. Robison. 2007b. Satellite-based Energy Balance for Mapping Evapotranspiration with Internalized Calibration (METRIC) -- Applications. *J. Irrig. and Drain. Engrg,* ASCE 133(4): 395-406.

ASCE-EWRI, 2005. The ASCE Standardized Reference Evapotranspiration Equation. Report of the ASCE-EWRI Task Committee on Standardization of Reference Evapotranspiration. 147 p.

Bastiaanssen, W.G.M. 1995. Regionalization of surface flux densities and moisture indicators in composite terrain: A remote sensing approach under clear skies in Mediterranean climates. Ph.D. dissertation, CIP Data Koninklijke Bibliotheek, Den Haag, The Netherlands. 273 p.

Bastiaanssen, W. G. M., Menenti, M., Feddes, R. A., and Holtslag, A. A. M. (1998). "A remote sensing surface energy balance algorithm for land (SEBAL): 1. Formulation." *J. Hydrol.*, 212–213, 198–212.

Majumdar, N.C., B.L. Mathur, and S.B. Kaushik. 1972. "Prediction of direct solar radiation for low atmospheric turbidity." *Solar Energy* 13: 383-394.

Tasumi M. 2003. Progress in operational estimation of regional evapotranspiration using satellite imagery. Ph.D. Dissertation, University of Idaho, Moscow, ID.

Tasumi, M., Allen, R.G., Trezza, R. and Wright, J.L. 2003. Soil Heat Flux Estimation Method. Appendix 12 of Tasumi (2003), Progress in operational estimation of regional evapotranspiration using satellite imagery. Ph.D. Dissertation, University of Idaho, Moscow, ID. (p 328-340).

Tasumi, M., R. Trezza , R.G. Allen and J. L. Wright. 2005. Operational aspects of satellite-based energy balance models for irrigated crops in the semi-arid U.S. *J. Irrigation and Drainage Systems.* 19 (3-4): 355-376.

Tasumi, M, R. G. Allen and Trezza, R. 2007. At-surface albedo from Landsat and MODIS satellites for use in energy balance studies of evapotranspiration, *Journal of Hydrolog. Eng*. (in press).

Trezza R. 2002. Evapotranspiration using a satellite-based surface energy balance with standardized ground control. Ph.D. Dissertation, Utah State University, Logan, UT.

Wukelic, G.E., D.E. Gibbons, et al., 1989. Radiometric calibration of Landsat thematic mapper thermal band. *Remote Sensing of Environment,* 28: 339-347.